# Physical and electrical characterization of bubble free transferred single crystal graphene

Soukaina Ben Salk, Reetu Raj Pandey, Phi Hq Pham, Di Zhou, Dominique Vignaud, Emiliano Pallecchi, Peter Burke, Henri Happy

# Physical and electrical characterization of bubble free transferred single crystal graphene

*Soukaina Ben Salk[1], Reetu Raj Pandey[1], Phi HQ Pham[2], Di Zhou[1], Dominique Vignaud[1], Emiliano pallecchi[1,*] , Peter J Burke[2], Henri Happy[1,*]*

[1]University of Lille - IEMN CNRS UMR8520, Avenue Poincaré, CS 60069, 59652 Villeneuve d'Ascq, France

[2]Department of Electrical Engineering and Computer Science, University of California, Irvine, CA 92697, USA

*Corresponding Authors: henri.happy@univ-lille.fr, emiliano.pallecchi@univ-lille.fr

**Abstract**

Monocrystalline graphene is desirable for practical applications since the large-scale polycrystalline graphene grown by chemical vapor deposition is limited in terms of performance. The transfer of graphene film from the metallic growth substrate to a host substrate, which is generally required for practical applications, can further damage the graphene by inducing strain, defects and wrinkles or by leaving contamination such as polymer residues. In this work, we have investigated the influence of the transfer process on the monocrystalline graphene in terms of quality, morphology and electrical properties by analyzing the data obtained from optical microscopy, scanning electron microscopy, Raman spectroscopy and electrical characterizations. The influence of copper oxidation on graphene prior to the transfer is also discussed. Our results show that the "Bubble-free" electrochemical delamination transfer is an easy and fast transfer technique suitable for transferring large single crystals graphene with an almost defect free surface. Moreover, Raman spectroscopy investigation reveals that the Cu surface oxidation modify the strain of the graphene film. We have observed that graphene laying on unoxidized Cu is submitted to a biaxial strain in compression, while graphene on Cu oxide is submitted to a biaxial strain in tension. However, after graphene was transferred to a host substrate, these strain effects disappeared leaving a homogeneous graphene on the substrate. Finally, we used the transferred single crystal graphene on silicon oxide substrate to fabricate transmission line method (TLM) devices. These electrical measurements show low contact resistance ~150 Ω.µm, which

confirms the homogeneity and good quality of transferred graphene. Therefore, electrochemical delamination process can be used to transfer large single crystal graphene in a fast and reliable way.
Keywords: monocrystalline graphene, electrochemical delamination, bubble-free transfer, Raman spectroscopy, defect-free, electrical characterization.

## 1. Introduction

Graphene with its extraordinary properties has dragged attention among the researchers to investigate its technological applications as graphene has high electrical and thermal conductivities, flexibility and stability.[1]–[7] Chemical vapor deposition (CVD) on copper has been broadly used to synthesize large-area and high-quality graphene.[8] Recently, the synthesis of large-area monocrystalline graphene has aroused interest among researchers to avoid the grain boundaries, responsible for graphene performance degradation. Because the majority of applications requires the as-grown graphene to be transferred to a host substrate, it is important to study how large monocrystalline domains behave during this process. Indeed, the transfer of graphene can have a considerable impact on its physical and electrical properties. [9][10]–[15] The transfer steps may damage the graphene film causing cracks, wrinkles and polymer residues and thus, reducing the carrier mobility of graphene, a parameter of the upmost importance for electronic applications.[16] Several methods have been developed to transfer the graphene from metal to the host substrates. The most common transfer technique involves the wet etching of the metal layer used as a catalyst template for the graphene growth, typically copper for monolayer graphene. This technique is reliable and well-studied [17]–[19], but has the disadvantage of a slow etching process, and destroying the copper film is non environmentally friendly. To overcome these limitations, remarkable progress has been made in the development of transfer techniques that avoid the etching of growth substrate. The most used method is the so-called electrochemical delamination transfer technique [4],[10]. Using this technique, few minutes are sufficient to separate the graphene layer from the growth substrate, compared to many hours required by the wet etching transfer method. Furthermore, this transfer technique significantly reduces metal consumption and the associated environmental pollution, and allows the reuse of the metal substrate, , [13], [20] which is especially promising for large-scale, low-cost production.

In this study, large isolated graphene monocrystals of millimeter scale dimensions (~5mm) have been synthesized on polycrystalline Cu foil [10]. After the growth, an annealing step was applied on some of the graphene-covered copper films to promote Cu oxidation. Afterwards, monocrystals of graphene, with and without post-growth oxidation, were transferred to $Si/SiO_2$ substrate using an optimized electrochemical delamination method. SEM and optical microscopy were used to analyze the morphology and quality of the material before and after transfer. Micro-Raman spectroscopy has been used to investigate how the oxidation of the copper underneath the graphene affects the graphene properties, by studying the strain and doping of the graphene films. Finally, transmission line measurement (TLM) structures were fabricated using the transferred graphene. Measurements performed on 6 TLM patterns, fabricated on a graphene single crystal, reveals a relatively low value of the contact resistance (~ 150 Ω.μm) which is attributed to the good quality of the transferred graphene and the fabrication process. The results presented in this work provide a path towards large-scale high-quality monocrystalline graphene transfer, which could contribute to the development of graphene-based electronic devices.

## 2. Experimental

This section briefly reminds the CVD synthesis of graphene on copper foils and details the transfer process of graphene samples.

### 2.1 Growth of large-size single crystal graphene

The synthesis of millimeter size monocrystal graphene - first reported in Ref.[11] - begins with an electrochemical polishing of the copper to improve the surface quality and thus decrease the nucleation density. The crystal growth is carried out inside enclosed copper pockets, to reduce the spreading of carbon and to slow the nucleation rate. The growth consists of two phases: a low methane flow is first employed during the nucleation phase to induce a low nucleus density, and the size of the crystals is enlarged from the nucleus in the second phase at an increased methane flow, as schematized in Fig. S1 in the supplementary information. Next, the copper pocket is unfolded and the as-grown sample (Fig. S2.a) is exposed to an intense flash light to identify the graphene crystals (Fig. S2.b). Latterly, the sample is annealed on a hot plate (250°C for 15 min) in order to oxidize the copper surface and to improve the visual contrast of graphene monocrystals, the size of which reaching 5 mm (see Fig. S3).

### 2.2. Electrochemical delamination transfer process of graphene (Bubble-free transfer)

Firstly, thin layer of 5% PMMA (polymethyl methacrylate) diluted in anisole was spin-coated onto graphene on one side of the Cu foil (3000 rpm, 1000 rpm/s, 10 s). Next, the sample (PMMA/graphene/Cu) was cured at 90°C for 30 min with very slow heating and cooling rates (30min), in order to prevent cracks in graphene caused by the strain induced in PMMA resist. Since the graphene was grown on both sides of the copper foil, the graphene on the back-side was removed by $O_2$ plasma etching (2min, 50W RF power) before being subjected to delamination.

Latterly, for electrochemical delamination "Bubble-free", PMMA/graphene/Cu stacks were immersed gradually in KOH solution (40 mmol/L) and a two-electrode system held at a potential of -2.7V. A continuous voltage was then applied between the cathode (the polymer/graphene/Cu sample) and anode (glassy carbon rod) in an electrolytic cell. KOH was used as the electrolyte solution and the decomposition of $H_2O$ causes the generation of $H_2$ bubbles at the Cu-graphene interface:

$$2H_2O\ (l) \rightarrow H_2\ (g) + 2OH\ (l)$$

$H_2$ bubbles help to separate graphene from the Cu surface. However, the uncontrolled production of hydrogen bubbles can cause mechanical damage in the graphene film. The complete delamination occurs within few minutes (less than 20 min). The graphene/PMMA film was then thoroughly rinsed (10 times) in deionized water to ensure the removal of residual KOH.

Finally, the graphene/PMMA film was transferred to $Si/SiO_2$ substrate and dried at 90°C for 30 min with very slow heating and cooling rates (30 min) in order to remove the water trapped underneath the graphene. The complete delamination and transfer process of graphene is presented in supporting figures S4 and S5 and the detailed optimization of the electrochemical delamination "Bubble-free" process is given in Supplementary Fig. S6. Scanning electron microscopy (SEM) images of the samples were taken with a Zeiss Ultra 55 SEM, equipped with a high efficiency lens. Raman spectrum were obtained with a confocal micro-Raman LabRam HR spectrometer (Horiba Jobin-Yvon) using an excitation laser (473 nm) focused with 100x objective.

## 3. Results and discussion

In this section, we present the detailed analysis of the bubble-free transfer process on the morphology and on the physical and electrical properties of the synthesized monocrystal of graphene.

### 3.1 Morphological and structural characterization of the as-grown single-crystal graphene

The synthesized graphene crystals were fully characterized before proceeding with the transfer. Two techniques were used, SEM and Raman spectroscopy as they can provide the local information on the structural uniformity and homogeneity of graphene samples. The SEM allows to image all the peculiarities of graphene**,** for example the shape of the synthesized crystals, grain boundaries and the presence of holes and discontinuities in the sheet of graphene. Fig. 1.a is an inverted contrast SEM image of a graphene sample after post-growth annealing in air. The hexagonal shape and the lack of observable grain boundaries suggest that the synthesized graphene is monocrystalline, which is confirmed by selected area electron diffraction (SAED) as reported in [10].

Fig. 1.c is a magnification of the area framed in Fig. 1.b, where we identify the three different contrasts which are pointed out by red, blue and black circles. The black circle refers to the oxidized copper substrate – free of graphene – and the red and blue circles correspond to the areas covered by the graphene film. In order to determine the source of the contrasts presented on the surface of the hexagonal domain, the areas marked by black, blue and red circles, and the edge of the graphene crystal (indicated by a green cross) have been studied by Raman spectroscopy. Fig. 2.a presents the typical Raman spectra corresponding to the different areas pointed in the SEM image of the Fig. 1.c with the respective colors. As expected, graphene peaks (G at ~1580 $cm^{-1}$ and 2D at ~2700$cm^{-1}$) are present in all areas except the black ones corresponding to the substrate. The blue spectrum in Fig. 2.a is the typical spectrum of a high-quality graphene monolayer on copper with $I_{2D}/I_G$ ~2. The red and green spectra also feature the G and 2D peaks, but have extra peaks between 900 $cm^{-1}$ and 1500 $cm^{-1}$ as represented in Fig. 2.c. It should be noticed that in the case of the red area, none of these peaks corresponds to the D peak (1349 $cm^{-1}$), a signature of structural defects in the graphene. The D peak is only observed at the edge of graphene (green cross in SEM image of the Fig. 2.a).

Thus, the absence of the D peak away from the edge of graphene as well as the presence of G and 2D peaks in areas pointed by the red and blue circles with an intensity ratio $I_{2D}/I_G > 2$ indicates that the graphene crystal is monolayer, homogeneous and of high quality. In Fig. 2.b, peaks below 900 $cm^{-1}$ are attributed to copper oxides (CuO and $Cu_2O$)[24]. These copper oxide peaks appear in the red and green spectra in Fig. 2.a and are absent in the blue area. These oxides are therefore the source of the contrast observed in the different areas of the graphene monolayer. The contrast is observed over the entire surface covered by graphene showing that the oxidation under graphene is not homogeneous. We can thus consider that the graphene crystal lays on two different substrates, copper and copper oxides.

### 3.2 Morphological characterization of single-crystal graphene on $SiO_2$ after transfer

The electrochemical delamination method described above was used to transfer the isolated large crystal graphene samples with and without air post-growth annealing. The optical images in Fig. 3 show the same graphene single crystals before and after transfer, confirming that the electrochemical transfer yields a homogeneous layer of graphene without tears or holes. This also demonstrates that the transfer process maintains the structure of graphene and should be achieved without damage.. To further analyze the oxidation effects of graphene crystals after post growth annealing, SEM investigations were carried out as shown in Fig. 4. Before transfer, the copper oxidation under graphene is non homogeneous as pointed out by the red arrows in Fig. 4.b which show areas where graphene stands on unoxydized copper. However, after the graphene transfer of this crystal, the surface of graphene looks uniform, keeping its original shape with no damage as seen in Fig. 4.c-d. This confirms that the transfer process does not depend on the oxidation of the Cu surface. The graphene layer after transfer remains homogeneous even though the oxydized Cu layer below the graphene was not. Analysis of the optical and SEM images shows that the “bubble-free” electrochemical delamination transfer process provides a homogeneous layer of graphene.

### 3.3 Characterization by Raman spectroscopy

Raman spectroscopy gives quantitative information on the quality of graphene. It allows to quantify the presence of structural defects, the level of graphene doping following the transfer and the evolution of stresses in the graphene layer. Four samples with and without post-growth annealing were studied and the Raman spectra of one of the sample measured after graphene transfer is depicted on Fig. 5.b. The presence of the G and 2D peaks and the absence of the D peak confirms the good quality of the transferred graphene.

Moreover, Raman measurements were carried out in different areas of the graphene crystal, leading to an average value of the intensity ratio $I_{2D}/I_G$ of ~3. This confirms that the graphene is monolayer thick and that it remains homogeneous after transfer. The full width at half maximum (FWHM) is ~ 29 $cm^{-1}$, which emphasizes the good quality of the crystal.

By comparing the Raman spectra of graphene before and after transfer (Fig. 5), it is noticed that the positions of the G and 2D peak shift (Table 1) depending on, whether the graphene lays on copper or on copper oxide. The shift of the peaks is directly linked to the strain and doping induced by the substrate [25] .

| | **Before transfer** | | **After transfer** |
|---|---|---|---|
| | *Graphene on copper* | *Graphene on Copper oxide* | *Graphene on $Si/SiO_2$* |
| **$\nu_G$ ($cm^{-1}$)** | 1591 ± 2 | 1579 ± 3 | 1590 ± 8 |
| **$\nu_{2D}$ ($cm^{-1}$)** | 2730 ± 2 | 2689 ± 3 | 2708 ± 10 |

*Table 1 Comparison of the positions of graphene's G and 2D peaks before and after transfer, from a Raman map of a graphene single crystal obtained from Fig. 6.*

### 3.4 Strain and doping profiles of graphene

This study is based on a vector decomposition method developed to study the influence of strain and doping on graphene as described in references [25], [26] . The variation in strain is studied before and after the transfer of graphene, considering the graphene on copper and graphene on copper oxide. Since the oxidation of copper under graphene is nonhomogeneous as described above (section 3.1 and 3.2), the Raman mapping is done on these two areas, with the “graphene on copper” and “graphene on copper oxide” as illustrated in the inset of Fig. 6(a) and in the supporting Fig. S7.

We have represented the frequency of the 2D peak as a function of the frequency of the G peak as shown in Fig. 6. The green cross in Fig. 6 represents the Raman peaks of undoped and unstrained graphene ($\nu_{G0=}1582cm^{-1}$, $\nu_{2D0=}2707cm^{-1}$) using an excitation laser at 473 nm. The blue line (biax. strain) represents a prediction of ($\nu_G$, $\nu_{2D}$) for an undoped graphene under biaxial stress. The orange line (p-doped) and the pink line (n-doped) represent predictions of ($\nu_G$, $\nu_{2D}$) for strain-free graphene under p or n charge doping respectively.

The Raman analysis of graphene samples before transfer (Fig. 6.a) shows the graphene laying on copper is under biaxial compressive strain (-0.34±0.03 %), whereas the graphene on copper oxide is subjected to a biaxial tensile strain of (0.3±0.1 %).

The Raman analysis is also done for four samples after graphene transfer (on $Si/SiO_2$) as shown in Fig. 6.b. 2 samples have been submitted to copper oxidation by air annealing after growth of graphene ("with post ox-sample1" and "with post ox-sample2"); and 2 others without any post-growth treatment ("Pristine-sample1" and "Pristine-sample2"). The Raman analysis alone cannot leads to any conclusion regarding the type of doping (n or p). But, from the literature which suggests that graphene transferred on $SiO_2$ is always p-doped [18], it is reasonable to assume that our samples are p-doped as well. Raman measurements have been obtained on different zones for each sample. The data (illustrated in Fig. 6.b) shows an evolution close to the orange line which represents a prediction of ($\nu_G$, $\nu_{2D}$) for strain-free graphene with p doping in the range $0 < p < 4.10^{12}$ $cm^{-2}$. Moreover, it can be seen that the graphene biaxial strain is almost completely relaxed after transfer onto $Si/SiO_2$ as shown in Fig. 6.b: the residual strain stands between -0.1 % and 0.16 % for all the samples. The obtained results are in good agreement with the reported literature [18], which shows that the monolayer graphene having a ratio $1 < I_{2D} / I_G < 2$ is highly doped.

### 3.5 Electrical characterization of single-crystal graphene after transfer

The TLM method was used to characterize the contact resistance as well as the sheet resistance of the graphene layer. We used single crystal graphene sample with copper oxidation by annealing in air before transfer. With this copper oxidation, the crystalline graphene samples become visible by eyes. Therefore, it is easy to select crystal for transfer. The interest of this oxidation step is to be able to choose easily what sample to use for transfer. The optical image of the device fabricated to measure the contact resistance is shown in the inset of Fig. 7.a. Ohmic contacts from six TLM patterns are obtained by analysing the linear behavior of the I-V curves. The resistances are then extracted and plotted as a function of the separation distance. Linear fitting is showing that variations in measured resistance are proportional to the separation distance between contacts and indicates the homogeneity of the graphene. Thus, we obtained a contact resistance RcW = 150Ωμm using Ni/Au contacts (with respective thickness of 1.5 nm and 50 nm), and a sheet resistance $\rho_{sh}$ = 797 Ω/square.

## 4. Conclusion

Large graphene single crystals up to a few millimeters were synthesized on copper substrates, and a reliable graphene transfer method ("Bubble-free transfer") has been developed. The applied potential and controlled generation of hydrogen bubbles play an important role in this electrochemical delamination approach. This transfer method is faster than the Cu wet chemical etching method (a few minutes versus a few hours). The quality of graphene is verified by different comparative pre- and post-transfer characterization approaches, including electrical, SEM and Raman spectroscopy.

We have also studied the impact of an extra post-growth annealing step on the copper oxidation on the large single-crystal graphene. The copper oxidation is non-uniform under the graphene crystals. The graphene on oxidized copper is under biaxial tension, whereas the areas where graphene is laying on non-oxidized copper exhibits biaxial compressive strain with a low doping. Moreover, after graphene was transferred to a host substrate, these strain effects disappear and the graphene doping varys depending on the host substrate. The electrical characterization of devices on a graphene single crystal shows a sheet resistance of $\rho_{sh}$ = 797 Ω/square and a contact resistance of 150 Ω.µm with Ni/Au contacts. Thus, the electrochemical delamination transfer process paves a path to easy and fast transfer of graphene maintaining its quality and its electrical properties.

## Acknowledgments: Renatech, flagship...

We acknowledge support from the Army Research Office through the ARO- (Contract No: W911NF-18-1-0076 and W911NF2010103), National Institutes of Health (Contract No: CA182384), the European Union's Horizon 2020 research and innovation program under phase of the Graphene Flagship GrapheneCore2 785219 and GrapheneCore3 881603 and the French American Cultural Exchange (FACE) Partner University Fund program. This work was also partly supported by the French RENATECH network

## References

[1] K. Cao *et al.*, « Elastic straining of free-standing monolayer graphene », *Nature Communications*, vol. 11, n° 1, déc. 2020, doi: 10.1038/s41467-019-14130-0.

[2] E. H. Hwang, S. Adam, et S. D. Sarma, « Carrier transport in 2D graphene layers », *Phys. Rev. Lett.*, vol. 98, n° 18, p. 186806, mai 2007, doi: 10.1103/PhysRevLett.98.186806.

[3] A. Balandin *et al.*, « Superior Thermal Conductivity of Single-Layer Graphene », *Nano letters*, vol. 8, p. 902‑7, avr. 2008, doi: 10.1021/nl0731872.

[4] S. Ghosh *et al.*, « Extremely High Thermal Conductivity of Graphene: Prospects for Thermal Management Applications in Nanoelectronic Circuits », *Applied Physics Letters*, vol. 92, p. 151911‑151911, avr. 2008, doi: 10.1063/1.2907977.

[5] C. Lee, X. Wei, J. Kysar, et J. Hone, « Measurement of the Elastic Properties and Intrinsic Strength of Monolayer Graphene », *Science (New York, N.Y.)*, vol. 321, p. 385‑8, juill. 2008, doi: 10.1126/science.1157996.

[6] A. A. Balandin, « Thermal properties of graphene and nanostructured carbon materials », *Nature Materials*, vol. 10, nº 8, Art. nº 8, août 2011, doi: 10.1038/nmat3064.

[7] R. R. Pandey *et al.*, « Tuning the electrical property of a single layer graphene nanoribbon by adsorption of planar molecular nanoparticles », *Nanotechnology*, vol. 28, nº 17, p. 175704, avr. 2017, doi: 10.1088/1361-6528/aa6567.

[8] W. Ren et H.-M. Cheng, « The global growth of graphene », *Nature Nanotechnology*, vol. 9, nº 10, p. 726‑730, oct. 2014, doi: 10.1038/nnano.2014.229.

[9] L.-P. Ma, W. Ren, et H.-M. Cheng, « Transfer Methods of Graphene from Metal Substrates: A Review », *Small Methods*, vol. 3, nº 7, juill. 2019, doi: 10.1002/smtd.201900049.

[10] P. H. Q. Pham, W. Zhou, N. V. Quach, J. Li, J.-G. Zheng, et P. J. Burke, « Controlling Nucleation Density While Simultaneously Promoting Edge Growth Using Oxygen-Assisted Fast Synthesis of Isolated Large-Domain Graphene », *Chemistry of Materials*, vol. 28, nº 18, p. 6511‑6519, sept. 2016, doi: 10.1021/acs.chemmater.6b01826.

[11] Y. Wu *et al.*, « Crystal Structure Evolution of Individual Graphene Islands During CVD Growth on Copper Foil », *Advanced Materials*, vol. 25, nº 46, p. 6744‑6751, déc. 2013, doi: 10.1002/adma.201302208.

[12] S. Chen *et al.*, « Millimeter-Size Single-Crystal Graphene by Suppressing Evaporative Loss of Cu During Low Pressure Chemical Vapor Deposition », *Advanced Materials*, vol. 25, nº 14, p. 2062‑2065, avr. 2013, doi: 10.1002/adma.201204000.

[13] L. Gao *et al.*, « Repeated growth and bubbling transfer of graphene with millimetre-size single-crystal grains using platinum », *Nature Communications*, vol. 3, nº 1, janv. 2012, doi: 10.1038/ncomms1702.

[14] S. Wu *et al.*, « Suitable Surface Oxygen Concentration on Copper Contributes to the Growth of Large Graphene Single Crystals », *The Journal of Physical Chemistry Letters*, vol. 10, nº 17, p. 4868‑4874, sept. 2019, doi: 10.1021/acs.jpclett.9b01688.

[15] X. Li *et al.*, « Large-Area Graphene Single Crystals Grown by Low-Pressure Chemical Vapor Deposition of Methane on Copper », *J. Am. Chem. Soc.*, vol. 133, nº 9, p. 2816‑2819, mars 2011, doi: 10.1021/ja109793s.

[16] Q. Yu *et al.*, « Control and characterization of individual grains and grain boundaries in graphene grown by chemical vapour deposition », *Nature Materials*, vol. 10, nº 6, Art. nº 6, juin 2011, doi: 10.1038/nmat3010.

[17] G. Deokar *et al.*, « Towards high quality CVD graphene growth and transfer », *Carbon*, vol. 89, p. 82‑92, août 2015, doi: 10.1016/j.carbon.2015.03.017.

[18] H. Park *et al.*, « Optimized poly(methyl methacrylate)-mediated graphene-transfer process for fabrication of high-quality graphene layer », *Nanotechnology*, vol. 29, n° 41, p. 415303, oct. 2018, doi: 10.1088/1361-6528/aad4d9.

[19] X. Li *et al.*, « Large-Area Synthesis of High-Quality and Uniform Graphene Films on Copper Foils », *Science*, vol. 324, n° 5932, p. 1312‑1314, juin 2009, doi: 10.1126/science.1171245.

[20] Y. Wang *et al.*, « Electrochemical Delamination of CVD-Grown Graphene Film: Toward the Recyclable Use of Copper Catalyst », *ACS Nano*, vol. 5, n° 12, p. 9927‑9933, déc. 2011, doi: 10.1021/nn203700w.

[21] C. J. L. de la Rosa *et al.*, « Frame assisted H2O electrolysis induced H2 bubbling transfer of large area graphene grown by chemical vapor deposition on Cu », *Appl. Phys. Lett.*, vol. 102, n° 2, p. 022101, janv. 2013, doi: 10.1063/1.4775583.

[22] G. Fisichella, S. Di Franco, F. Roccaforte, S. Ravesi, et F. Giannazzo, « Microscopic mechanisms of graphene electrolytic delamination from metal substrates », *Appl. Phys. Lett.*, vol. 104, n° 23, p. 233105, juin 2014, doi: 10.1063/1.4882165.

[23] S. Koh, Y. Saito, H. Kodama, et A. Sawabe, « Epitaxial growth and electrochemical transfer of graphene on Ir(111)/α-Al2O3(0001) substrates », *Appl. Phys. Lett.*, vol. 109, n° 2, p. 023105, juill. 2016, doi: 10.1063/1.4958843.

[24] S. Karle *et al.*, « Synthesis and evaluation of new copper ketoiminate precursors for a facile and additive-free solution-based approach to nanoscale copper oxide thin films », *Dalton Trans.*, vol. 46, n° 8, p. 2670‑2679, févr. 2017, doi: 10.1039/C6DT04399B.

[25] J. E. Lee, G. Ahn, J. Shim, Y. S. Lee, et S. Ryu, « Optical separation of mechanical strain from charge doping in graphene », *Nature Communications*, vol. 3, n° 1, janv. 2012, doi: 10.1038/ncomms2022.

[26] F. Fromm, P. Wehrfritz, M. Hundhausen, et T. Seyller, « Looking behind the scenes: Raman spectroscopy of top-gated epitaxial graphene through the substrate », *New Journal of Physics*, vol. 15, n° 11, p. 113006, nov. 2013, doi: 10.1088/1367-2630/15/11/113006.

**Figures**

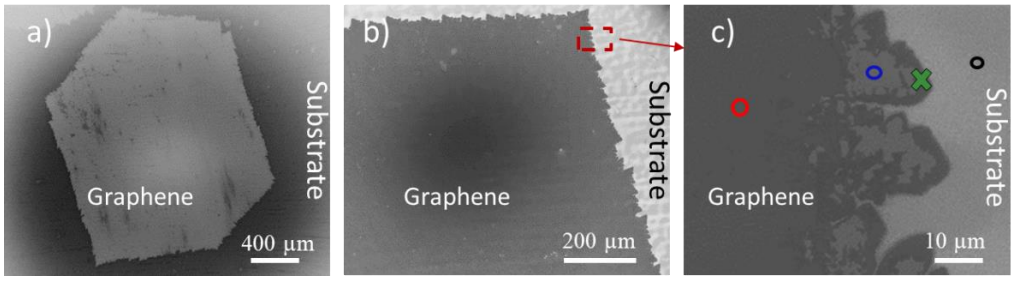


Fig. 1: Graphene monocrystal with post-growth annealing before transfer, (a) SEM image of a hexagonal monocrystal (b) edge of the graphene monocrystal, (c) magnified area framed in red in panel b, showing one graphene edge close to which Raman spectra were measured (colored marks).

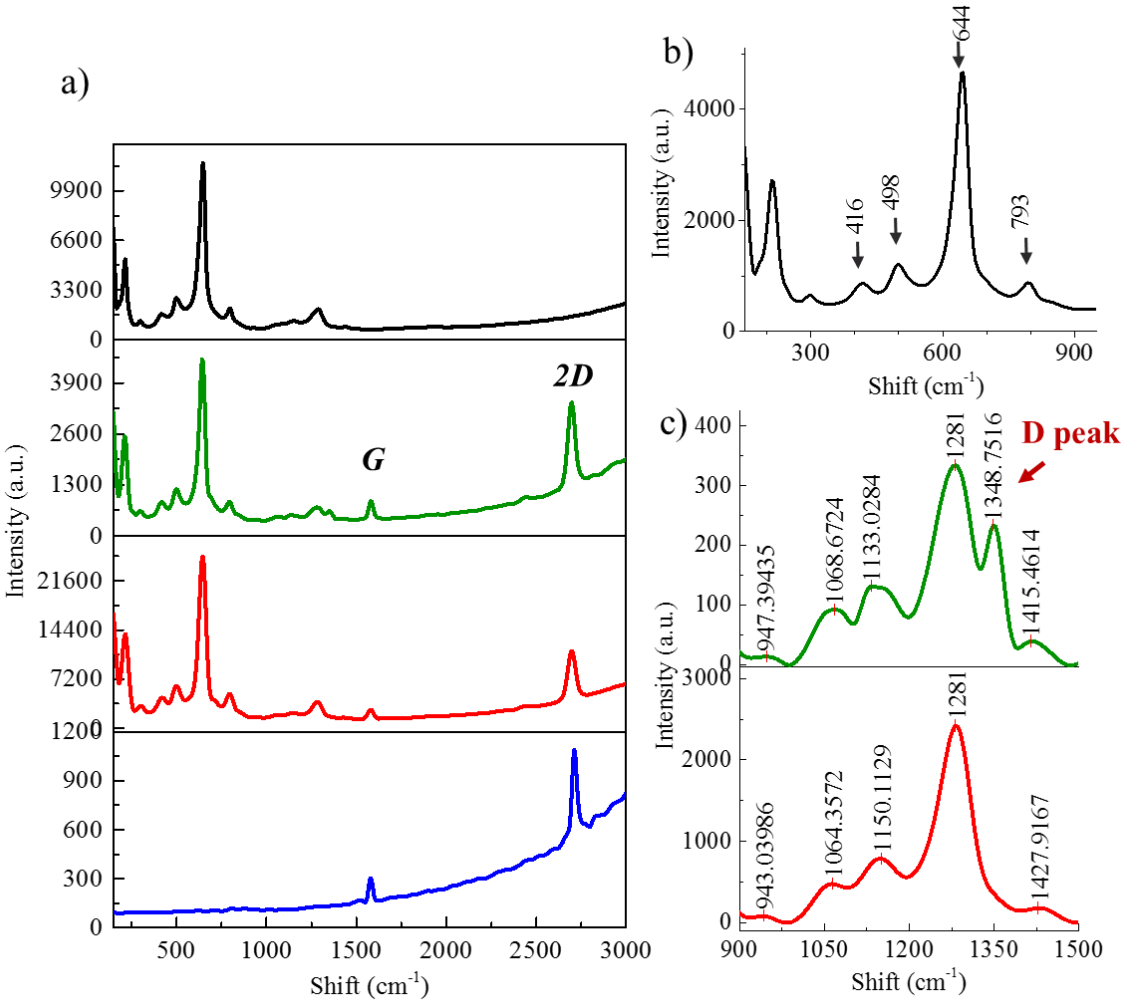


Fig. 2: (a) Raman spectra corresponding to areas pointed in Fig. 1.c using the same colors, (b) zoom-in between 0 and 900 $cm^{-1}$ of the black spectrum showing copper oxide peaks and (c) zoom-in between 900 $cm^{-1}$ and 1500 $cm^{-1}$ for the red and green spectra of panel a.

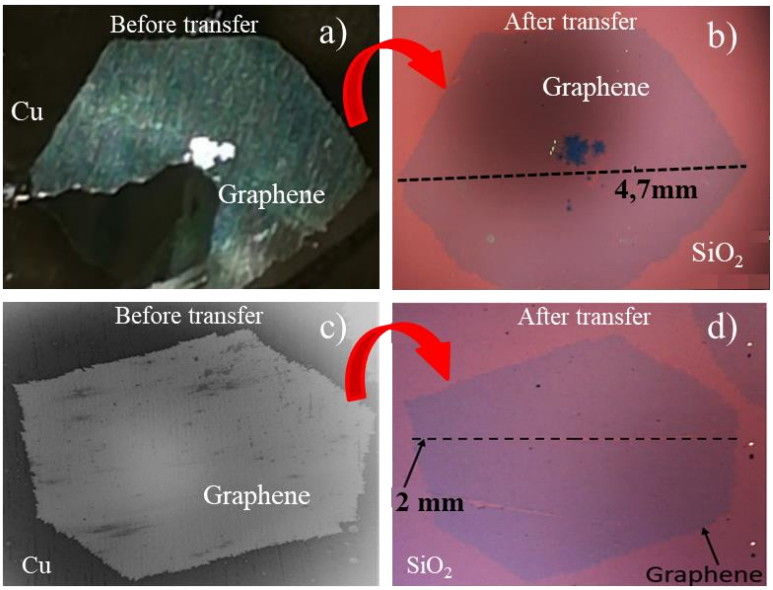


Fig. 3: Images of single crystal graphene, (a-b) optical image sample without annealing before (a) and after bubble-free transfer (b), (c-d) SEM and optical images of large single crystal graphene transferred to $SiO_2$ substrate sample with post-growth annealing before (c) and after transfer (d), SEM images (a, c) and optical images (b, d).

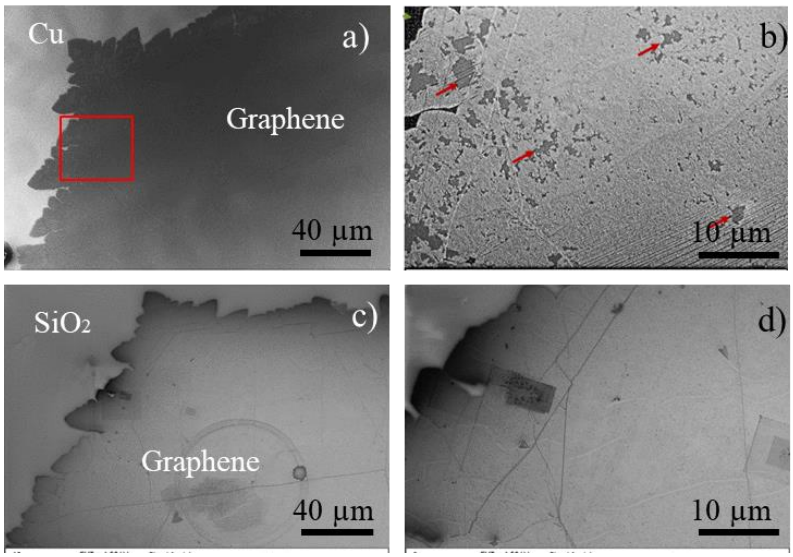


Fig. 4: SEM images of graphene samples with post growth annealing (a-b) before transfer, (b) magnification of red square in panel a, red arrows pointing the unoxidized Cu areas, (c-d) same area after transfer, the graphene is homogeneous.

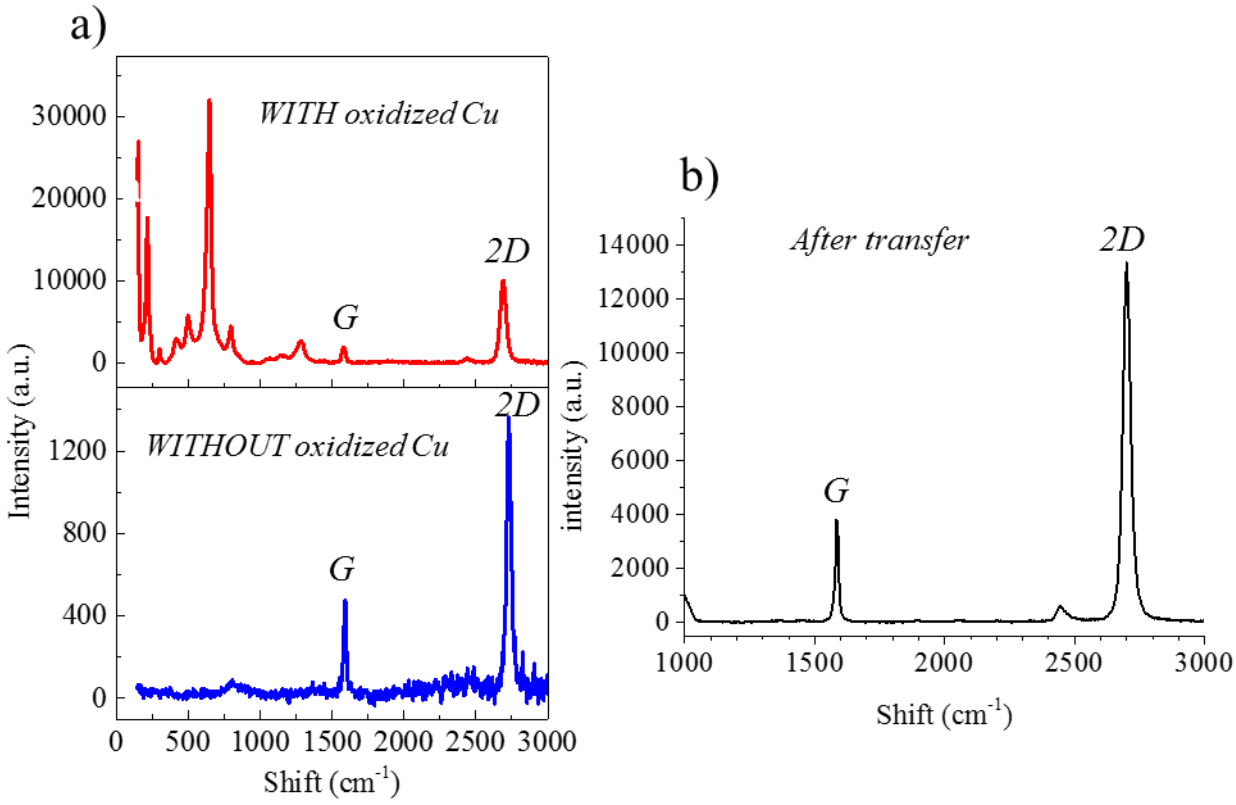


Fig. 5: Raman spectra of graphene from Fig. 1.c after subtracting the baseline. (a) Red represents an area where graphene is on copper oxide, blue represents an area where graphene is on copper. Both spectra are obtained on the same graphene crystal (b) after transfer on $SiO_2$.

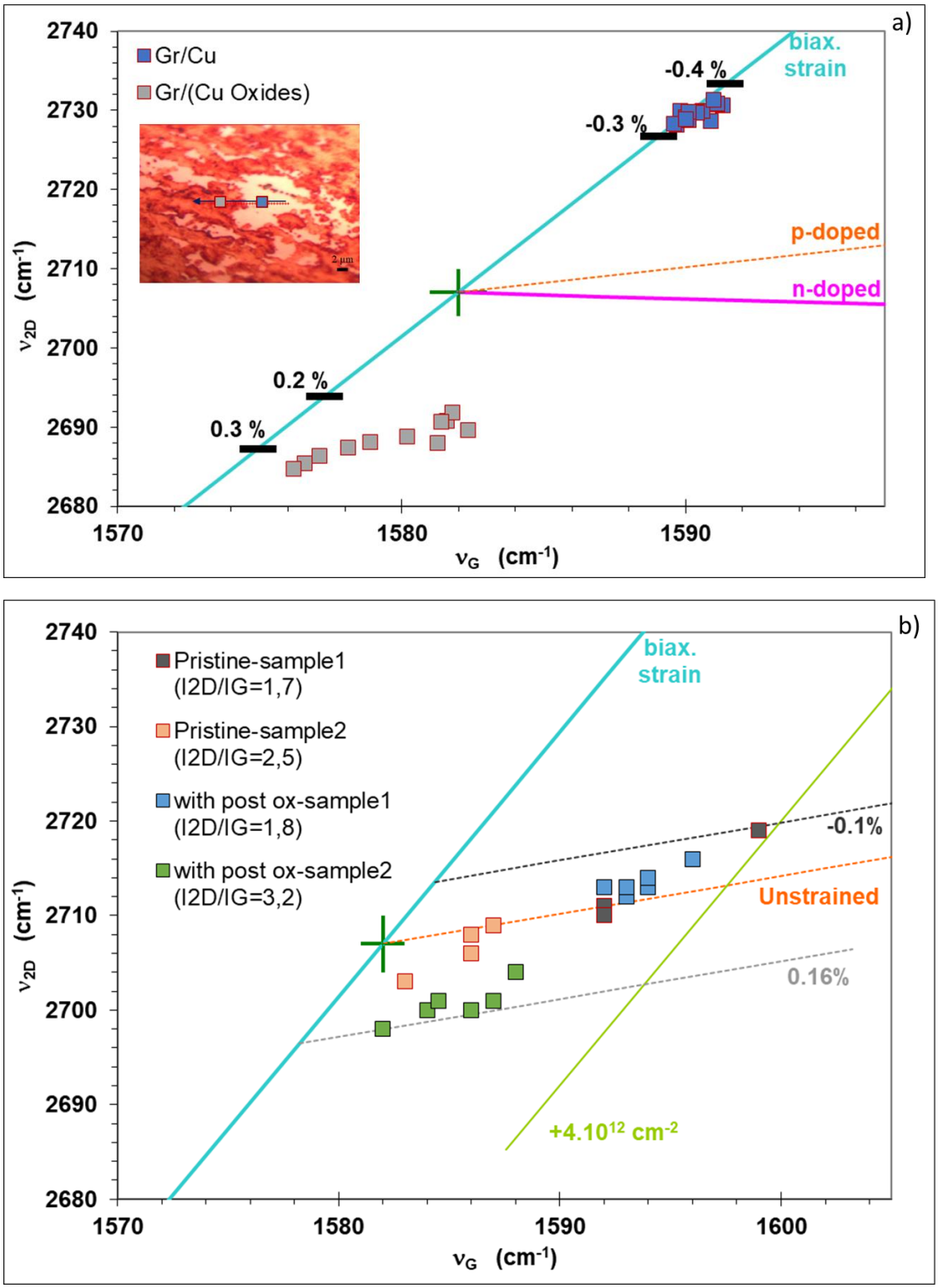


Fig. 6: Correlation between the frequencies of the G and 2D Raman peaks of graphene ($\nu_G$,$\nu_{2D}$), from Raman spectra of 4 samples, with and without post-growth annealing. The green cross represents ($\nu_{G0}$,$\nu_{2D0}$) for undoped and unstrained graphene. The blue line (biax. strain) represents an estimation of ($\nu_G$,$\nu_{2D}$) for undoped graphene under biaxial strain, while the orange (respectively pink) dashed line corresponds to unstrained p-doped (n-doped) graphene. Horizontal black lines in panel a refer to the values of biaxial strain. (a) before transfer, (b) after transfer, the green line parallel to the blue one represents the ($\nu_G$,$\nu_{2D}$)strain dependency for a p-type doping of $4.10^{12}$ cm$^{-2}$.

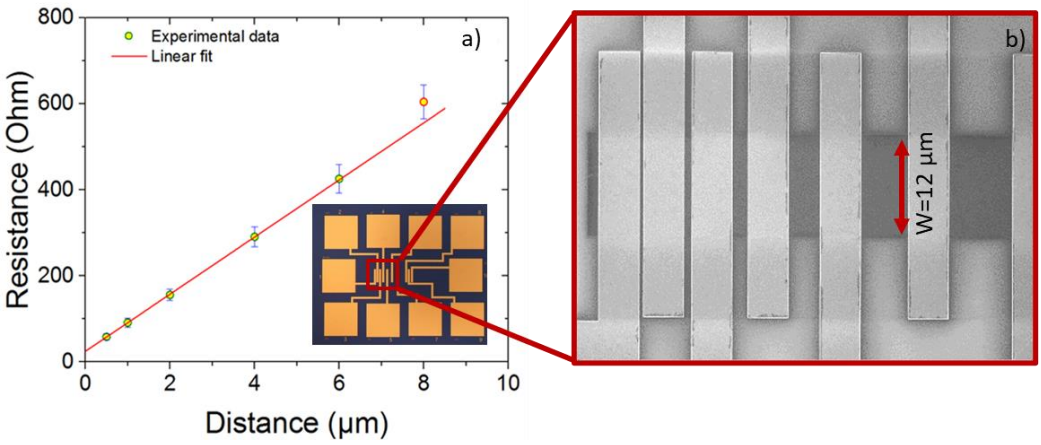


Fig. 7: (a) Plot of resistance with TLM structure for a graphene width of 12 μm, inset is an optical image of a TLM structure (b) SEM image showing a magnification of the framed area in the inset